

Hydrophobic Polyoxometalate-Based Metal-Organic Framework for Efficient CO₂ Photoconversion

Xiao-Xin Li,^{†,‡} Jiang Liu,[‡] Lei Zhang,[‡] Long-Zhang Dong,^{‡,§} Zhi-Feng Xin,^{‡,§} Shun-Li Li,[‡] Xue-Qing Huang-Fu,[‡] Kai Huang,^{*,†,§} and Ya-Qian Lan^{*,‡,§}

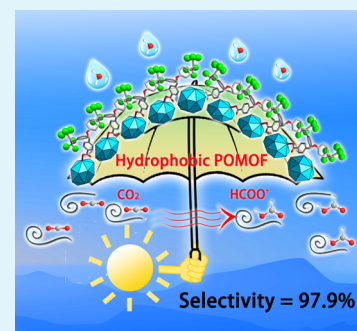
[†]School of Chemistry and Chemical Engineering, Southeast University, Nanjing 211189, P. R. China

[‡]Jiangsu Collaborative Innovation Centre of Biomedical Functional Materials, Jiangsu Key Laboratory of New Power Batteries, College of Chemistry and Materials Science, Nanjing Normal University, Nanjing 210023, P. R. China

[§]Institute of Molecular Engineering and Applied Chemistry, Anhui University of Technology, Ma'anshan 243002, P. R. China

S Supporting Information

ABSTRACT: A novel polyoxometalate (POM)-based metal-organic framework, TBA₅[P₂Mo₁₆^VMo₈^{VI}O₇₁(OH)₉Zn₈(L)₄] (NNU-29), was in situ synthesized and applied into CO₂ photoreduction. The selection of porous material containing a reductive POM cluster is considered to be helpful for CO₂ reduction; meanwhile, a hydrophobic-group-modified organic ligand enables NNU-29 to exhibit good chemical stability and restrains hydrogen generation to some extent. In the photocatalytic CO₂ reduction, the yield of HCOO[−] reached 35.2 μmol in the aqueous solution with selectivity of 97.9% after 16 h.



KEYWORDS: polyoxometalate-based metal-organic frameworks, hydrophobicity, structural stability, heterogeneous catalyst, carbon dioxide photoreduction

1. INTRODUCTION

The burning of fossil fuels leads to excessive carbon dioxide emission into the atmosphere, causing serious environmental and energy problems that need to be solved urgently.^{1–3} Photocatalytic reduction of CO₂ into value-added chemicals or hydrocarbon fuels in water to simulate natural photosynthesis can slow down the process of energy consumption and reduce CO₂ concentration.^{4–8} However, the chemical inertness of the CO₂ molecule makes it difficult to be activated and converted, which requires effective catalysts with reducibility to participate in this process and accomplish it. Moreover, as a competitive reaction, the hydrogen evolution reaction always reduces the selectivity of the photocatalytic reaction. Not only does it wear out portion of the photogenerated electrons for CO₂ conversion, but also it is disadvantageous for further separation and purification of the target product. Therefore, it is a goal to construct reductive photocatalysts to convert CO₂ with high selectivity.

Metal-organic frameworks (MOFs) have been widely investigated in the fields of gas adsorption and catalysis over the decades due to their structural controllability and open catalytic sites.^{9–12} Meanwhile, the appropriate spatial structure of MOFs can help understand the catalysis mechanism at the molecular level.^{13–16} It is noticed that the secondary building units, which always play the role of a catalytic center, directly determine the efficiency of the catalytic reaction, mostly. Introducing reductive nodes to construct MOFs can result in a

great performance in some reduction reactions.^{17–20} It is well-known that polyoxometalates (POMs) and their derivatives show outstanding properties in plenty of catalytic reactions, in which POMs function as high-efficiency catalytic sites with splendid redox ability and semiconductor characters.^{21–24} Nevertheless, simple POM clusters are often soluble in water, so it is difficult to recycle them and they may cause environmental pollution. Therefore, stability is the prerequisite for POM-based derivatives as heterogeneous catalysts. It is noted that when connecting POMs with linkers to construct polyoxometalate-based metal-organic frameworks (POMOFs), they can not only retain the advantages of POMs but also keep stable in aqueous solution.²⁵ This indicates a potential method to select reductive POMs like {Zn₄P₂Mo₈^VMo₄^{VI}} or {Mo₆^VO₁₂(OH)₃(HPO₄)₃(PO₄)₃}²⁶ to synthesize POMOFs as photocatalysts, which may have beneficial effects on CO₂ reduction.

Based on the above considerations, we combined POM and a hydrophobic ligand to synthesize a stable POM-based metal-organic framework, TBA₅[P₂Mo₁₆^VMo₈^{VI}O₇₁(OH)₉Zn₈(L)₄] (NNU-29; L^{2−} is 4,4'-(((perfluoropropane-2,2-diyl)bis(4,1-phenylene)))bis(oxy))bis(methylene)dibenzoate anion and TBA⁺ is the tetrabutylammonium ion). With the help of a

Received: March 4, 2019

Accepted: June 26, 2019

Published: June 26, 2019

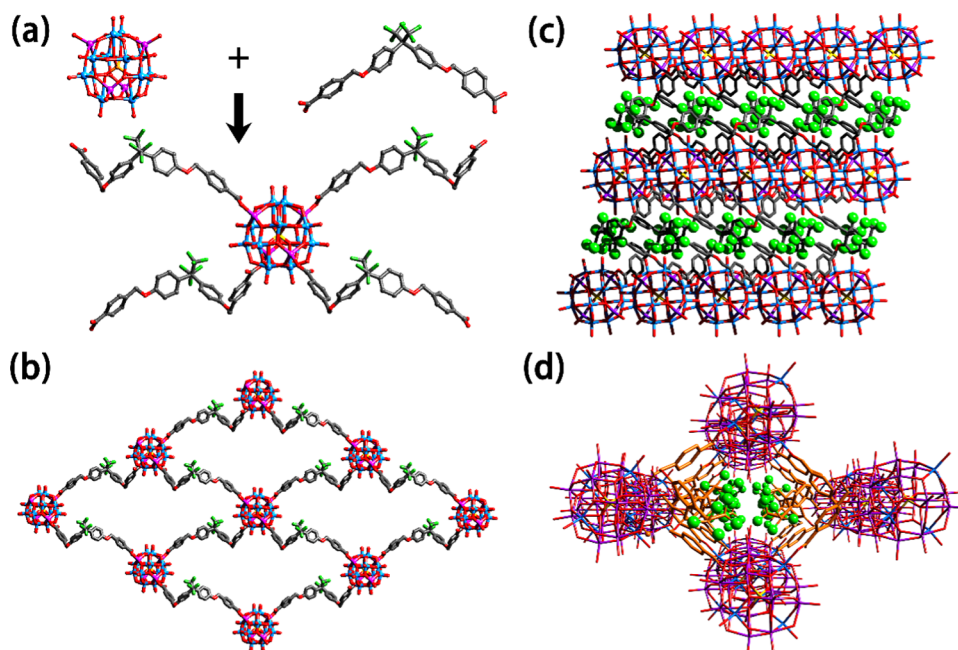


Figure 1. Summary of the structure of NNU-29: (a) Coordination environments of NNU-29; all hydrogen atoms are omitted for clarity. P, yellow; Mo, light blue; Zn, violet; C, gray; O, red; N, blue; and F, green. (b) The single 2D layer network along the *c*-axis. (c) POM layers and trifluoromethyl layers form a sandwich-like structure along the *b*-axis. (d) A rhombic channel full of trifluoromethyl along the *c*-axis.

fluorine-containing ligand, NNU-29 shows strong hydrophobicity and chemical stability. It is noticed that introducing the $\{Zn_4PMo_8^{VI}Mo_4^{VI}\}$ unit with strong reducibility into the structure enables NNU-29 to perform efficient heterogeneous photocatalytic conversion of CO_2 to $HCOOH$ in water. The $HCOOH$ production is $220 \mu mol g^{-1} h^{-1}$ along with the selectivity of nearly 98%. The existence of a fluorine-containing ligand avoids the attack from water to generate H_2 to some degree.

2. EXPERIMENTAL SECTION

2.1. Synthesis of $TBA_5[P_2Mo_{16}^{VI}Mo_8^{VI}O_{71}(OH)_9Zn_8(L)_4]$ (NNU-29). A mixture of $Na_2MoO_4 \cdot 2H_2O$ (0.600 g, 2.50 mmol), H_3PO_3 (0.020 g, 0.25 mmol), $ZnCl_2$ (0.20 g, 1.47 mmol), and H_2O (6.0 mL) was stirred for 1 h, resulting in a milky white suspension. Then, molybdenum powder (60 mg, 0.62 mmol) and H_2L (0.063 g, 0.10 mmol) were introduced. TBAOH (25 wt %) in methanol (0.1 mL, 0.09 mmol) and HCl (0.2 mL, 6.0 M) was added to adjust the pH of the aqueous suspension. The solution was mixed under vigorous stirring, ultrasound-treated for approximately 30 min, and transferred and sealed in a 15 mL Teflon-lined stainless steel container maintained at $180^\circ C$ for 72 h and then cooled to room temperature for more than 24 h. Dark red rhombus crystals of NNU-29 (Figure S2) were separated and washed with Millipore water, which were collected in 40% yield based on H_2L . The CCDC reference number is 1893141. Synthesis procedures of H_2L and $Zn_4\epsilon$ -Keggin are given in the Supporting Information.

2.2. Photocatalytic Test. The photocatalytic CO_2 reduction experiments were carried out on an evaluation system (CEL-SPH2N, CEAULIGHT, China) in a 100 mL quartz container. A 300 W xenon arc lamp with a UV-cutoff filter (420–800 nm) was utilized as the irradiation source. The photocatalysts (NNU-29, $Zn_4\epsilon$ -Keggin or H_2L) were dispersed in 50 mL solution, and pre-degassed with CO_2 (99.999%) for 30 min to remove air before irradiation. The reaction mixture was kept stirred constantly with a magnetic bar to ensure complete mixing of the photocatalyst particles in suspension. The temperature of the reaction was maintained at $20^\circ C$ by a circulating cooling water system.

3. RESULTS AND DISCUSSION

X-ray crystallography reveals that NNU-29 crystallized in the monoclinic space group $C2/c$ and with two formula units ($Z = 2$) per unit cell (Table S2). NNU-29 consists of the ϵ - $\{Zn_4PMo_{12}O_{40}\}$ cluster as the inorganic building node, the hydrophobic fluorine-based ligand as the linker, and TBA^+ ions. The secondary building unit can be considered as ϵ - $\{PMo_{12}O_{40}\}$ capped by four Zn ions in tetrahedral symmetry.^{27–30} There are four Mo(VI) and eight Mo(V) in one $\{Zn_4PMo_{12}O_{40}\}$ cluster, indicating that the Keggin node is a reductive POM (Figure S14b). Each grafted Zn ion coordinates with the carboxylic oxygen from a flexible L^{2-} ligand to generate a two-dimensional (2D) network, which is shown in Figure 1a. Besides, regarding the ϵ - $\{Zn_4PMo_{12}O_{40}\}$ cluster as a 4-connected node, the skeletons of NNU-29 feature a topology with the Schläfli symbol of $4^4 \cdot 6^2$, which reveals the topology of the sql code. Figure 1b shows the layer network along the *c*-axis. In fact, the authentic layer contains three independent interpenetrating frameworks, which are shown in Figure S4.

The contact angle of H_2L is measured to be 133.68° (Figure S1), which shows that it is a hydrophobic ligand. What is interesting and worth noting in the structure is that all of the locations of trifluoromethyl are around the POM node, which can protect the hydrophilic POMs, avoiding the attack from H_2O . Along the *b*-axis, POMs and trifluoromethyl are likely to be two kinds of layers interlaced together to form a sandwich-like structure (Figure 1c). In the view along the *c*-axis, four rows of POMs leave a rhombic channel, which is full of trifluoromethyl (Figure 1d). In the interspace, TBA^+ ions act as counteranions to balance the charges. Because of the above-mentioned factors, NNU-29 shows hydrophobic characteristics. The result of contact angle measurement was 122° , which evidences NNU-29 as hydrophobic (Figure 2a).

The introduction of hydrophobic ligands results in NNU-29 exhibiting good hydrophobic properties and acid–base

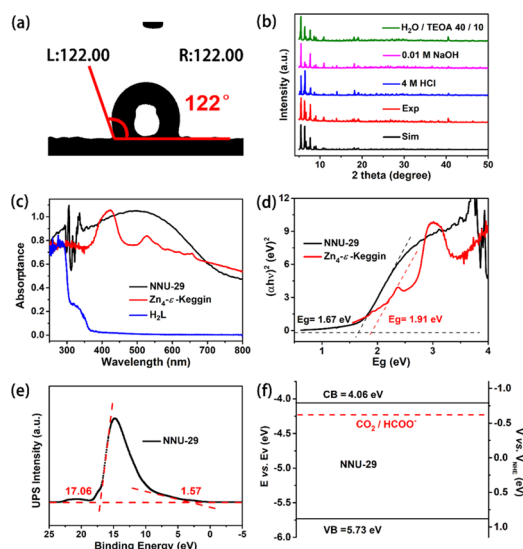


Figure 2. (a) Contact angle measurement of NNU-29. Both the left and right angles are 122°. (b) Powder X-ray diffraction (PXRD) patterns of NNU-29 in different solutions compared with simulated curves. (c) UV-vis absorption of NNU-29 (black curve), $\text{Zn}_4\text{-}\epsilon\text{-Keggin}$ (red curve), and H_2L (blue curve). (d) $(\alpha h\nu)^2$ vs $h\nu$ curve of NNU-29 (black curve) and $\text{Zn}_4\text{-}\epsilon\text{-Keggin}$ (red curve). (e) Ultraviolet photoelectron spectroscopy (UPS) spectra of NNU-29. (f) Band structure diagram for NNU-29.

stability. Phase purity of single-crystal NNU-29 was determined by well-matched powder X-ray diffraction (PXRD) patterns (Figure 2b). The chemical stability measurements were performed by soaking prepared samples in aqueous solution for 48 h under different conditions. The consistent peaks reveal that NNU-29 can remain crystalline in 4 M HCl and 0.01 M NaOH solution. The structural integrity of NNU-

29 in triethanolamine (TEOA) solution (1:4, v/v) provides long-term durability during CO_2 photoreduction process as catalysts directly. This rigid structure exhibits superior chemical stability, which is fairly rare among most MOFs and POMOFs.

The thermal stability of NNU-29 was examined through thermogravimetric analysis. As shown in Figure S7, there is no significant change in thermal weight before 300 °C, indicating that NNU-29 has good thermodynamic stability. The 46.71% weight loss of NNU-29 from 300 to 680 °C is attributed to the splitting of TBA^+ ions and the release of L^{2-} ligand, calculated to be 46.44%.

$\text{TBA}_4[\text{PMo}_8^{\text{VI}}\text{Mo}_4^{\text{VI}}\text{O}_{37}(\text{OH})_3\text{Zn}_4]\text{Cl}_4$ ($\text{Zn}_4\text{-}\epsilon\text{-Keggin}$), the inorganic node of NNU-29, was further synthesized,³¹ and its properties were studied. Suggested by the ultraviolet–visible (UV–vis) results shown in Figure 2c, NNU-29 reveals broad UV–vis light absorption covering the entire UV–visible light region. On comparing the absorption of $\text{Zn}_4\text{-}\epsilon\text{-Keggin}$ and pure H_2L , it can be firmly believed that the absorption is mainly contributed by the $\epsilon\text{-}\{\text{Zn}_4\text{PMo}_{12}\text{O}_{40}\}$ cluster. The band gaps (E_g) of NNU-29 and $\text{Zn}_4\text{-}\epsilon\text{-Keggin}$ were further calculated from original UV–vis data with the Kubelka–Munk formula: $(\alpha h\nu = C(h\nu - E_g)^2)$. In Figure 2d, the intersection of the tangent lines from the curve and horizontal lines shows that the band gaps are 1.67 and 1.91 eV for NNU-29 and $\text{Zn}_4\text{-}\epsilon\text{-Keggin}$, respectively. To confirm the position of the valence band (VB) of NNU-29, ultraviolet photoelectron spectroscopy (UPS) was performed (Figure 2e). The result was ultimately calculated to be 5.73 eV by deducting the width of the He I UPS spectra from the excitation energy (21.22 eV). Then, the position of the conduction band was evaluated to be 4.06 eV by $E_v - E_g$. What is revealed in Figure 2f is the band structure of NNU-29. The values of bending coefficient (CB) and VB were converted to the normal hydrogen electrode

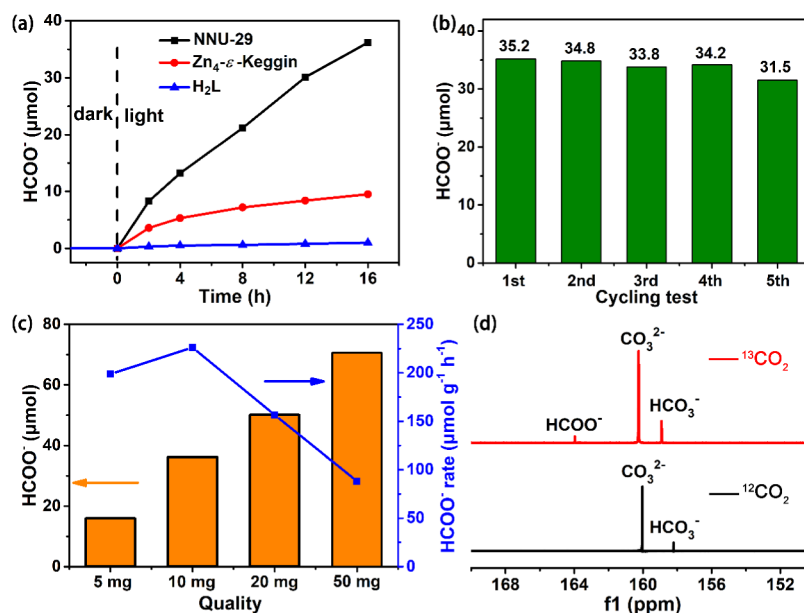


Figure 3. (a) Amount of HCOO^- produced as a function of the time of visible-light irradiation over NNU-29, $\text{Zn}_4\text{-}\epsilon\text{-Keggin}$, and H_2L . The reaction with each photocatalyst (10 mg) in the $\text{H}_2\text{O}/\text{TEOA}$ (4:1 v/v, 50 mL) solution was irradiated using a Xe lamp filtered to produce light in the range of 420–800 nm; (b) the evolution of HCOO^- produced in five consecutive runs (recovery of the used catalyst and then redispersed in a fresh photosensitizer solution for 16 h in each run) of the photocatalytic CO_2 reaction over NNU-29; (c) the effect of different quantities of NNU-29 on the yield (left) and rate (right) of HCOO^- from the CO_2 photoreduction system; and (d) ^{13}C NMR spectra of the product obtained from the reaction with $^{13}\text{CO}_2$ (red) and $^{12}\text{CO}_2$ (black).

(NHE) in volts (right y-axis). The reduction potential of CO_2/HCOOH is lower than the conduction band of NNU-29, which indicates that it can be a photocatalyst for CO_2 -to- HCOOH reduction theoretically. To further confirm the semiconductor band structure, the Mott–Schottky plot measurement on NNU-29 was implemented at frequencies of 1000, 1500, and 2000 Hz. As shown in Figure S8, the obtained C^{-2} curves with the x-axis were intersected at -0.76 V vs Ag/AgCl. Then, the position of the CB was further calculated to be -0.66 V vs NHE, which agreed with the result of UPS.

In addition, NNU-29 has a distinguished transient photocurrent response under visible-light irradiation when the light is “turn on” or “turn off” (Figure S9). The sensitive photocurrent response of NNU-29 represented a high separating efficiency of photoinduced electron–hole pairs. It is important to note that NNU-29 has been proven to be a semiconductor material with a conduction band-edge potential that matched the theoretical reduction potential required by HCOO^- .

In the system of CO_2 photoreduction, triethanolamine (TEOA) as the sacrificial agent and $[\text{Ru}(\text{bpy})_3]\text{Cl}_2 \cdot 6\text{H}_2\text{O}$ (11.2 mg, 0.0134 mmol) as the supporting photosensitizer (PS) were introduced. It is a widely approved approach to improve the performance.^{32,33} Because of the appropriate lowest unoccupied molecular orbital (LUMO) positions between catalysts and PS (Figure S10), photo-motivated electrons were allowed to transfer from PS to catalysts. As we expected, NNU-29 reveals noteworthy photocatalytic performances for CO_2 reduction. By testing the yield of HCOO^- at 4, 8, 12, and 16 h, respectively, we achieve a roughly linear relationship between the target product and the reaction time (Figure 3a). The amount grew to $35.20 \mu\text{mol}$ in 16 h, which corresponded to a turnover number (TON) (Table 1) of 28.09

Table 1. Research of Reaction Conditions for NNU-29^a

entry	HCOOH (μmol)	CO (μmol)	CH_4 (μmol)	H_2 (μmol)	TON	selectivity (%)
1	35.2	0.18	0.58	n.d.	28.09	97.9
2 ^{bD}	n.d.	n.d.	n.d.	n.d.		
3 ^c	n.d.	0.76	n.d.	0.68		
4 ^d	n.d.	1.85	n.d.	n.d.		
5 ^e	7.5	2.45	0.25	0.4	3.39	70.7
6 ^f	0.8	n.d.	n.d.	n.d.	0.048	
7 ^g	6.4	1.56	0.19	n.d.		78.5
8 ^h	n.d.	n.d.	n.d.	n.d.		

^aReaction conditions: NNU-29 (10 mg, $1.28 \mu\text{mol}$), $[\text{Ru}(\text{bpy})_3]\text{Cl}_2 \cdot 6\text{H}_2\text{O}$ (11.2 mg, $13.4 \mu\text{mol}$), solvent (50 mL, $\text{H}_2\text{O}/\text{TEOA}$, 4/1), CO_2 (1 atm), $\lambda \geq 420$ nm, 20 °C, 16 h reaction time; n.d. = not detectable; turnover number (TON) = $(n(\text{HCOOH}) + n(\text{CO}) + n(\text{CH}_4) + n(\text{H}_2))/n(\text{photocatalyst})$; selectivity = $(n(\text{HCOOH}))/n(\text{HCOOH} + n(\text{CO}) + n(\text{CH}_4) + n(\text{H}_2)) \times 100\%$, where $n(\text{HCOO}^-)$ and $n(\text{photocatalyst})$ were the amounts of HCOO^- (mol) and the catalyst (mol), respectively. ^{bD}Dark condition. ^cNo catalyst. ^dNo $[\text{Ru}(\text{bpy})_3]\text{Cl}_2 \cdot 6\text{H}_2\text{O}$. ^eZn-ε-keggins replaced NNU-29. ^f H_2L replaced NNU-29. ^gPhysical mixture of Zn-ε-keggins and H_2L to replace NNU-29. ^hAr replaced CO_2 .

for HCOO^- formation. There were no any other products detected in the liquid. A little amount of CO ($0.18 \mu\text{mol}$) and CH_4 ($0.58 \mu\text{mol}$) gas production (Figure S11) was detected by gas chromatography (Figure S17). In addition, no affiliated H_2 produced during the entire reaction (Figure S18). The results above indicated a high selectivity up to 97.9% for CO_2

photoreduction. In addition, NNU-29 can be easily recovered from the test reaction solution by centrifugation. After removing the supernatant liquid, the catalyst was washed with water three times. The sample was dried in the air for the next round. As shown in Figure 3b, NNU-29 can keep the original activity of ca. 90% after five cycles. The PXRD patterns (Figure S12), Fourier transform infrared spectroscopy (Figure S13), and X-ray photoelectron spectroscopy (Figure S14a) showed no significant changes before and after the cycle experiment, which proved the structural stability of NNU-29 again.

The effect of the quantity of NNU-29 on the photochemical performance of the system was further studied. As shown in Figure 3c, the amount of HCOO^- produced was increasing along with the increase in the amount of NNU-29. When 5 mg of NNU-29 was introduced into the system, $15.90 \mu\text{mol}$ of HCOO^- was produced corresponding to a rate of $198.75 \mu\text{mol g}^{-1} \text{h}^{-1}$. When the amount increased to 10 mg, the rate of HCOO^- formation reached the highest value of $220 \mu\text{mol g}^{-1} \text{h}^{-1}$. Even though the yield of HCOO^- enhanced along with the greater quantity of photocatalysts, the formation rate of HCOO^- decreased sharply. It could be ascribed to the rate-determining step of the process, which was the transfer of photoelectron from PS to NNU-29. The redundant catalyst did not serve completely due to the limited generation of photoelectron.³⁴

To investigate the active roles of CO_2 photoreduction, a series of contrast experiments were conducted, and the results are listed in Table 1. When the experiment was carried out in the dark (entry 2), no any products were detected either in gas or liquid, indicating that it is a light-driven catalytic reaction. When the experiment was carried out in lack of NNU-29, no HCOO^- but little CO and H_2 could be observed (entry 3). In the absence of $[\text{Ru}(\text{bpy})_3]\text{Cl}_2 \cdot 6\text{H}_2\text{O}$, the efficiency of CO_2 reduction decreased dramatically and only trace of CO can be detected (entry 4). The result showed that the photoelectrons excited from PS and NNU-29 might be the active centers in the photocatalysis process. To further confirm where the catalysis reaction happens, the properties of pure Zn₄-ε-keggins (entry 5) or H_2L (entry 6) were examined. Contrastively, Zn₄-ε-keggins revealed performance of $7.5 \mu\text{mol}$ production, indicating that the exact catalysis center is the ε- $\{\text{Zn}_4\text{P}(\text{Mo}_{12}\text{O}_{40})\}$ cluster. In the homogeneous system consisting of H_2L , $[\text{Ru}(\text{bpy})_3]\text{Cl}_2 \cdot 6\text{H}_2\text{O}$, and TEOA, almost the same yield as that in entry 4 showed the insertion of ligand. Then, the physical mixture of Zn₄-ε-keggins and H_2L was used to replace NNU-29 (entry 7). The result showed an obvious but weaker activity than that of NNU-29, revealing that the fluorine-containing network of NNU-29 promoted the effect on CO_2 conversion.^{35,36} The participation of CO_2 in the reaction was also studied by replacing CO_2 with Ar (entry 8). There is no carbonaceous substance detected, which indicates that the HCOO^- was transformed from CO_2 . Furthermore, an isotopic $^{13}\text{CO}_2$ experiment was carried out. The production of HCOO^- was analyzed by ^{13}C NMR spectroscopy. As shown in Figure 3d, when using $^{12}\text{CO}_2$ as a carbon source, the peaks corresponding to TEOA and deuterium-dimethyl sulfoxide were easily found in the ^{13}C NMR spectrum from the filtrate after reaction. In the range from 158 to 166 ppm, two weak peaks at 158.2 and 159.9 could be due to HCO_3^{2-} and CO_3^{2-} , respectively, for the large solubility of CO_2 and the alkaline environment due to the existence of TEOA to form these ions. When $^{13}\text{CO}_2$ was employed in the reaction system, a new and

obvious peak appeared at 163.9 ppm, which corresponds to the HCOO^- ion, which strongly indicates that the produced HCOO^- indeed transformed from CO_2 . Overall, these results have demonstrated the main role of NNU-29 acting as a CO_2 redox promoter in the photocatalytic reduction system. For comparison, we have listed the performance of a series of other metal-organic compounds as the photocatalysts for CO_2 -to- HCOOH conversion in the Supporting Information (Table S6).

Upon analyzing the experimental facts and theoretical calculation (Figure S21), a speculative reaction mechanism in regard to photocatalytic CO_2 -to- HCOOH reduction over NNU-29 was proposed (Figure 4). First, the photosensitizer

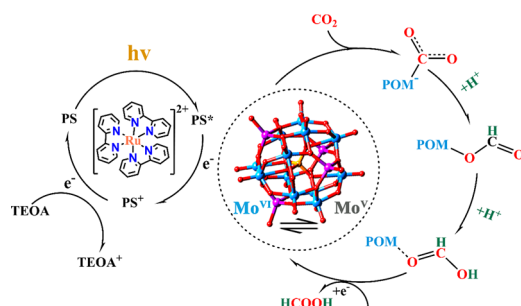


Figure 4. Proposed mechanism for the photocatalytic reduction of CO_2 to HCOOH photocatalyzed by NNU-29.

$[\text{Ru}(\text{bpy})_3]^{2+}$ absorbs visible light. Photoelectrons are excited from highest occupied molecular orbital to LUMO and then transferred to the catalyst NNU-29 through the matched LUMO positions. NNU-29 is like an electronic sponge and receives photoelectrons due to the valence change of multiple Mo ions. Second, reductive POM units play a vital role in capturing and reducing CO_2 and then convert back into original photocatalysis. TEOA as an electron donor consumes the photoinduced holes produced in the valence band of $[\text{Ru}(\text{bpy})_3]^{2+}$.

4. CONCLUSIONS

In summary, a novel POMOF (NNU-29) with a two-dimensional sandwich plane structure was reported. Due to the introduction of a hydrophobic ligand, NNU-29 exhibits high chemical stability. $\epsilon\text{-}\{\text{Zn}_4\text{POM}_{12}\text{O}_{40}\}$, a cluster with outstanding reducibility, prompts NNU-29 to show outstanding property as a heterogeneous catalyst for CO_2 photoreduction under visible-light irradiation. Meanwhile, hydrophobicity depresses the evolution of hydrogen to some degree, which guarantees the high selectivity of CO_2 -to- HCOO^- conversion (97.9%). The relation between the structure and properties of NNU-29 is a successful case for designing efficient catalysts with contemporary selectivity. It is expected that a rational tactics to design a stable structure with reductive inorganic clusters and functional ligands by reasonable synthesis strategies will have a significant impact on increasing the activity and selectivity in CO_2 photoreduction.

■ ASSOCIATED CONTENT

Supporting Information

The Supporting Information is available free of charge on the ACS Publications website at DOI: 10.1021/acsami.9b03861.

Crystallographic data, NNU-29 (CIF)

Materials and measurements; analytical techniques; single-crystal X-ray diffraction; electrochemical measurements and computation; synthesis of $\text{L}(\text{OMe})_2$, H_2L ; the Mott–Schottky plot and the photocurrent of NNU-29; PXRD before and after reactions of NNU-29 and $\text{Zn}_4\text{-}\epsilon\text{-keggin}$; ^{13}C NMR spectrum; ion chromatograph and gas chromatography analysis after CO_2 photoreduction; and theoretical calculation detail (PDF)

■ AUTHOR INFORMATION

Corresponding Authors

*E-mail: huangk@seu.edu.cn (K.H.).

*E-mail: yqlan@njnu.edu.cn (Y.-Q.L.).

ORCID

Long-Zhang Dong: 0000-0002-9276-5101

Kai Huang: 0000-0002-5768-4189

Ya-Qian Lan: 0000-0002-2140-7980

Author Contributions

The manuscript was written through contributions of all authors. All authors have given approval to the final version of the manuscript.

Notes

The authors declare no competing financial interest.

■ ACKNOWLEDGMENTS

The authors are grateful to the financial aid from the NFSC (Nos. 21622104, 21871141, 21871142, 21576049, and 21701085), the NSF of Jiangsu Province of China (Nos. SBK2017040708 and BK20171032), the Natural Science Research of Jiangsu Higher Education Institutions of China (No. 17KJB150025), Priority Academic Program Development of Jiangsu Higher Education Institutions, and the Foundation of Jiangsu Collaborative Innovation Center of Biomedical Functional Materials.

■ REFERENCES

- (1) Steinlechner, C.; Junge, H. Renewable Methane Generation from Carbon Dioxide and Sunlight. *Angew. Chem., Int. Ed.* **2017**, *57*, 44–45.
- (2) Inoue, T.; Fujishima, A.; Konishi, S.; Honda, K. Photoelectrocatalytic Reduction of Carbon Dioxide in Aqueous Suspensions of Semiconductor Powders. *Nature* **1979**, *277*, 637–638.
- (3) Mikkelsen, M.; Jørgensen, M.; Krebs, F. C. The teraton challenge. A Review of Fixation and Transformation of Carbon Dioxide. *Energy Environ. Sci.* **2010**, *3*, 43–81.
- (4) Quadrelli, E. A.; Centi, G. Green Carbon Dioxide. *ChemSusChem* **2011**, *4*, 1179–1181.
- (5) Rao, H.; Schmidt, L. C.; Bonin, J.; Robert, M. Visible-Light-Driven Methane Formation from CO_2 with a Molecular Iron Catalyst. *Nature* **2017**, *548*, 74–77.
- (6) Stone, E. J.; Lowe, J. A.; Shine, K. P. The Impact of Carbon Capture and Storage on Climate. *Energy Environ. Sci.* **2009**, *2*, 81–91.
- (7) Hull, J. F.; Himeda, Y.; Wang, W.-H.; Hashiguchi, B.; Periana, R.; Szalda, D. J.; Muckerman, J. T.; Fujita, E. Reversible Hydrogen Storage Using CO_2 and a Proton-switchable Iridium Catalyst in Aqueous Media under Mild Temperatures and Pressures. *Nat. Chem.* **2012**, *4*, 383–388.
- (8) Tamaki, Y.; Watanabe, K.; Koike, K.; Inoue, H.; Morimoto, T.; Ishitani, O. Development of Highly Efficient Supramolecular CO_2 Reduction Photocatalysts with High Turnover Frequency and Durability. *Faraday Discuss.* **2012**, *155*, 115–127.
- (9) Liu, Q.; Cong, H. J.; Deng, H. X. Deciphering the Spatial Arrangement of Metals and Correlation to Reactivity in Multivariate Metal–Organic Frameworks. *J. Am. Chem. Soc.* **2016**, *138*, 13822–13825.

- (10) Wang, X.; Wissler, F. M.; Canivet, J.; Fontecave, M.; Mellot-Draznieks, C. Immobilization of a Full Photosystem in the Large Pore MIL101 Metal-Organic Framework for CO₂ Reduction. *ChemSusChem* **2018**, *11*, 3315–3322.
- (11) Liao, P. Q.; Huang, N. Y.; Zhang, W. X.; Zhang, J. P.; Chen, X. M. Controlling Guest Conformation for Efficient Purification of Butadiene. *Science* **2017**, *356*, 1193–1196.
- (12) Zhang, H.; Nai, J.; Yu, L.; Lou, X. W. Metal-Organic-Framework-Based Materials as Platforms for Renewable Energy and Environmental Applications. *Joule* **2017**, *1*, 77–107.
- (13) Dhakshinamoorthy, A.; Asiri, A. M.; García, H. Metal–Organic Framework (MOF) Compounds: Photocatalysts for Redox Reactions and Solar Fuel Production. *Angew. Chem., Int. Ed.* **2016**, *55*, S414–S445.
- (14) Li, N.; Liu, J.; Liu, J.-J.; Dong, L.-Z.; Xin, Z.-F.; Teng, Y.-L.; Lan, Y.-Q. Adenine Components in Biomimetic Metal–Organic Frameworks for Efficient CO₂ Photoconversion. *Angew. Chem., Int. Ed.* **2019**, *58*, S226–S231.
- (15) Xu, H. Q.; Hu, J.; Wang, D.; Li, Z.; Zhang, Q.; Luo, Y.; Yu, S. H.; Jiang, H. L. Visible-Light Photoreduction of CO₂ in a Metal–Organic Framework: Boosting Electron–Hole Separation via Electron Trap States. *J. Am. Chem. Soc.* **2015**, *137*, 13440–13443.
- (16) Luo, T.; Zhang, J.; Li, W.; He, Z.; Sun, X.; Shi, J.; Shao, D.; Zhang, B.; Tan, X.; Han, B. Metal-Organic Framework Stabilized CO₂/Water Interfacial Route for Photocatalytic CO₂ Conversion. *ACS Appl. Mater. Interfaces* **2017**, *9*, 41594–41598.
- (17) Moghadam, P. Z.; FairenJimenez, D.; Snurr, R. Q. Efficient Identification of Hydrophobic MOFs: Application in the Capture of Toxic Industrial Chemicals. *J. Mater. Chem. A* **2016**, *4*, 529–536.
- (18) Ding, N.; Li, H.; Feng, X.; Wang, Q.; Wang, S.; Ma, L.; Zhou, J.; Wang, B. Partitioning MOF-5 into Confined and Hydrophobic Compartments for Carbon Capture under Humid Conditions. *J. Am. Chem. Soc.* **2016**, *138*, 10100–10103.
- (19) Mukherjee, S.; Kansara, A. M.; Saha, D.; Gonnade, R.; Mullangi, D.; Manna, B.; Desai, A. V.; Thorat, S. H.; Singh, P. S.; Mukherjee, A.; Ghosh, S. K. An Ultrahydrophobic Fluorous Metal–Organic Framework Derived Recyclable Composite as a Promising Platform to Tackle Marine Oil Spills. *Chemistry* **2016**, *22*, 10937–10943.
- (20) Rana, S.; Rajendra, R.; Dhara, B.; Jha, P. K.; Ballav, N. Highly Hydrophobic and Chemically Rectifiable Surface-Anchored Metal-Organic Framework Thin-Film Devices. *Adv. Mater. Interfaces* **2016**, *3*, No. 1500738.
- (21) Hu, J.; Ji, Y.; Chen, W.; Streb, C.; Song, Y. “Wiring” redox-active Polyoxometalates to Carbon Nanotubes using a Sonication-driven Periodic Functionalization Strategy. *Energy Environ. Sci.* **2016**, *9*, 1095–1101.
- (22) Li, T.; Wang, Z.; Chen, W.; Miras, H. N.; Song, Y. F. Rational Design of a Polyoxometalate Intercalated Layered Double Hydroxide: Highly Efficient Catalytic Epoxidation of Allylic Alcohols under Mild and Solvent-Free Conditions. *Chem. Eur. J.* **2017**, *23*, 1069–1077.
- (23) Song, Y. F.; Tsunashima, R. Recent Advances on Polyoxometalate-based Molecular and Composite Materials. *Chem. Soc. Rev.* **2012**, *41*, 7384–7402.
- (24) Ji, Y.; Huang, L.; Hu, J.; Streb, C.; Song, Y. F. Polyoxometalate-functionalized Nanocarbon Materials for Energy Conversion, Energy Storage and Sensor Systems. *Energy Environ. Sci.* **2015**, *8*, 776–789.
- (25) Du, D. Y.; Qin, J. S.; Li, S. L.; Su, J. M.; Lan, Y. Q. Recent Advances in Porous Polyoxometalate-Based Metal-Organic Framework Materials. *Chem. Soc. Rev.* **2014**, *43*, 4615–4632.
- (26) Xie, S. L.; Liu, J.; Dong, L. Z.; Li, S. L.; Lan, Y. Q.; Su, Z. M. Hetero-Metallic Active Sites Coupled with Strongly Reductive Polyoxometalate for Selective Photocatalytic CO₂-to-CH₄ Conversion in Water. *Chem. Sci.* **2018**, *10*, 185–190.
- (27) Rousseau, G.; Rodriguez-Albelo, L. M.; Salomon, W.; Mialane, P.; Marrot, J.; Doungmene, F.; Mbomekallé, I. I.-M.; de Oliveira, P.; Dolbecq, A. Tuning the Dimensionality of Polyoxometalate-Based Materials by Using a Mixture of Ligands. *Cryst. Growth Des.* **2015**, *15*, 449–456.
- (28) Rodriguez-Albelo, L. M.; Ruiz-Salvador, A. R.; Sampieri, A.; Lewis, D. W.; Gómez, A.; Nohra, B.; Mialane, P.; Marrot, J.; Sécheresse, F.; Mellot-Draznieks, C.; Ngo Biboum, R.; Keita, B.; Nadjo, L.; Dolbecq, A. Zeolitic Polyoxometalate-Based Metal-Organic Frameworks (Z-POMOFs): Computational Evaluation of Hypothetical Polymorphs and the Successful Targeted Synthesis of the Redox-Active Z-POMOF1. *J. Am. Chem. Soc.* **2009**, *131*, 16078–16087.
- (29) Nohra, B.; El Moll, H.; Rodriguez Albelo, L. M.; Mialane, P.; Marrot, J.; Mellot-Draznieks, C.; O’Keeffe, M.; Ngo Biboum, R.; Lemaire, J.; Keita, B.; Nadjo, L.; Dolbecq, A. Polyoxometalate-Based Metal Organic Frameworks (POMOFs): Structural Trends, Energetics, and High Electrocatalytic Efficiency for Hydrogen Evolution Reaction. *J. Am. Chem. Soc.* **2011**, *133*, 13363–13374.
- (30) Rodriguez Albelo, L. M.; Ruiz-Salvador, A. R.; Lewis, D. W.; Gómez, A.; Mialane, P.; Marrot, J.; Dolbecq, A.; Sampieri, A.; Mellot-Draznieks, C. Zeolitic Polyoxometalates Metal Organic Frameworks (Z-POMOF) with Imidazole Ligands and ϵ -Keggin Ions as Building Blocks; Computational Evaluation of Hypothetical Polymorphs and a Synthesis Approach. *Phys. Chem. Chem. Phys.* **2010**, *12*, 8632–8639.
- (31) Qin, J. S.; Du, D. Y.; Guan, W.; Bo, X. J.; Li, Y. F.; Guo, L. P.; Su, Z. M.; Wang, Y. Y.; Lan, Y. Q.; Zhou, H. C. Ultrastable Polymolybdate-Based Metal–Organic Frameworks as Highly Active Electrocatalysts for Hydrogen Generation from Water. *J. Am. Chem. Soc.* **2015**, *137*, 7169–7177.
- (32) Tamaki, Y.; Morimoto, T.; Koike, K.; Ishitani, O. Photocatalytic CO₂ Reduction with High Turnover Frequency and Selectivity of Formic Acid Formation Using Ru(II) Multinuclear Complexes. *Proc. Natl. Acad. Sci. U.S.A.* **2012**, *109*, 15673–15678.
- (33) Lefebvre, J.-F.; Schindler, J.; Traber, P.; Zhang, Y.; Kupfer, S.; Gräfe, S.; Baussanne, I.; Demeunynck, M.; Mouesca, J.-M.; Gambarelli, S.; Artero, V.; Dietzek, B.; Chavarot-Kerlidou, M. An artificial photosynthetic system for photoaccumulation of two electrons on a fused dipyrrophenazine (dppz)–pyridoquinolinone ligand. *Chem. Sci.* **2018**, *9*, 4152–4159.
- (34) Wang, S.; Yao, W.; Lin, J.; Ding, Z.; Wang, X. Cobalt Imidazolate Metal-Organic Frameworks Photosplit CO₂ under Mild Reaction Conditions. *Angew. Chem., Int. Ed.* **2014**, *53*, 1034–1038.
- (35) Pan, F.; Li, B.; Xiang, X.; Wang, G.; Li, Y. Efficient CO₂ Electroreduction by Highly Dense and Active Pyridinic Nitrogen on Holey Carbon Layers with Fluorine Engineering. *ACS Catal.* **2019**, *9*, 2124–2133.
- (36) Wang, Y.; Chen, J.; Wang, G.; Li, Y.; Wen, Z. Perfluorinated Covalent Triazine Framework Derived Hybrids for the Highly Selective Electroconversion of Carbon Dioxide into Methane. *Angew. Chem., Int. Ed.* **2018**, *57*, 13120–13124.